Reproductive Biology and Endocrinology

RESEARCH

Open Access

Identification of energy metabolism anomalies and serum biomarkers in the progression of premature ovarian failure via extracellular vesicles' proteomic and metabolomic profiles

Zhen Liu[1,2], Qilin Zhou[2], Liangge He[3], Zhengdong Liao[2], Yajing Cha[2], Hongyu Zhao[2], Wenchao Zheng[2], Desheng Lu[4] and Sheng Yang[2*]

Abstract

Background Premature ovarian failure (POF) is a clinical condition characterized by the cessation of ovarian function, leading to infertility. The underlying molecular mechanisms remain unclear, and no predictable biomarkers have been identified. This study aimed to investigate the protein and metabolite contents of serum extracellular vesicles to investigate underlying molecular mechanisms and explore potential biomarkers.

Methods This study was conducted on a cohort consisting of 14 POF patients and 16 healthy controls. The extracellular vesicles extracted from the serum of each group were subjected to label-free proteomic and unbiased metabolomic analysis. Differentially expressed proteins and metabolites were annotated. Pathway network clustering was conducted with further correlation analysis. The biomarkers were confirmed by ROC analysis and random forest machine learning.

Results The proteomic and metabolomic profiles of POF patients and healthy controls were compared. Two subgroups of POF patients, Pre-POF and Pro-POF, were identified based on the proteomic profile, while all patients displayed a distinguishable metabolomic profile. Proteomic analysis suggested that inflammation serves as an early factor contributing to the infertility of POF patients. For the metabolomic analysis, despite the dysfunction of metabolism, oxidative stress and hormone imbalance were other key factors appearing in POF patients. Signaling pathway clustering of proteomic and metabolomic profiles revealed the progression of dysfunctional energy metabolism during the development of POF. Moreover, correlation analysis identified that differentially expressed proteins and metabolites were highly associated, with six of them being selected as potential biomarkers. ROC curve analysis, together with random forest machine learning, suggested that AFM combined with 2-oxoarginine was the best diagnostic biomarker for POF.

*Correspondence:
Sheng Yang
tobyys2000@aliyun.com

Full list of author information is available at the end of the article

Conclusions Omics analysis revealed that inflammation, oxidative stress, and hormone imbalance are factors that damage ovarian tissue, but the progressive dysfunction of energy metabolism might be the critical pathogenic pathway contributing to the development of POF. AFM combined with 2-oxoarginine serves as a precise biomarker for clinical POF diagnosis.

Keywords POF, Extracellular vesicles, Proteomics, Metabolomics, Biomarker

Background

Premature ovarian failure (POF) is a disease affecting approximately 1% of females before they reach 40 years of age, resulting in the cessation of the menstrual cycle and infertility [1]. The underlying mechanisms causing POF are not comprehensively understood, although hormonal imbalances, genetic mutations, environmental factors, and autoimmune diseases have been shown to contribute to POF development [2–5]. Presently, the diagnosis of POF relies on measuring the serum levels of follicle-stimulating hormone (FSH) and estradiol [6], as well as clinical manifestations. However, the progression of POF is gradual, and reliable biomarkers for early diagnosis and prognostication during the initial stages of the disease are currently lacking. There is a need for more specific and sensitive biomarkers to enable early-stage diagnosis of POF.

In recent years, technological advancements have enabled the identification of proteins and metabolites in biological fluids, furnishing novel insights into disease etiology and diagnostics. Proteomic analysis involves the identification of the total protein component of the biological sample, including both soluble and membrane-bound proteins. This method facilitates the identification and quantification of alterations in protein expression levels, post-translational modifications, and protein interactions [7]. Conversely, metabolomic analysis characterizes the metabolomic profile of the biological sample, including small molecule metabolites such as amino acids, lipids, and nucleotides. This approach enables the identification of changes in metabolic pathways associated with a particular disease or condition [8]. Proteomic and metabolomic analyses both serve as powerful tools for identifying biomarkers in various diseases, including neurological disorders, cardiovascular disease, and cancer [9–12]. These methods also hold promise for understanding the underlying mechanisms of POF and identifying novel biomarkers for its diagnosis and treatment. Previous studies have utilized the serum component as a biomarker for POF due to its conventionality [13, 14], but the complexity of serum constituents limits its specificity [15].

Extracellular vesicles are believed to play a critical role in intercellular communication, and the analysis of their proteomic content has been utilized to investigate the underlying physiological and pathological processes, including cancer, inflammation, and immune responses [16]. In recent years, several studies have explored exosomal content to develop therapies or diagnostic biomarkers for female reproductive diseases. A recent study identified the miRNA profile in plasma extracellular vesicles, suggesting several signaling pathways contributing to the development of polycystic ovarian syndrome (PCOS), and proposed their potential utility as biomarkers to distinguish patients from controls [17]. Another study identified the miRNA profile in endometriosis and suggested that miR-22-3p and miR-320a could serve as noninvasive diagnostic biomarkers [18]. To date, there are no existing data illustrating the exosomal content in serum from POF patients, but the use of serum extracellular vesicles is promising for understanding the underlying molecular mechanisms of POF, and its use as a noninvasive diagnostic biomarker. To date, there are currently no studies that reveal the differences in the cargo of serum extracellular vesicles between patients with POF and healthy individuals. As a result, there is a lack of understanding of the pathogenesis of POF from the perspective cell communication regulated by extracellular vesicles, and it is also impossible to use blood to more accurately diagnose the occurrence of POF. This study aims to address this issue by analyzing the protein and metabolites content in the extracellular vesicles isolated from serum.

In this study, we constructed exosomal proteomic and metabolomic profiles derived from the serum of POF patients. The quantification of proteins and metabolites, including their downstream regulatory signals, associated environmental factors, and interactions, provides clues for diagnosing and treating POF. Furthermore, omic analysis revealed interplay between proteins and metabolites, with key nodes in the network being discovered. We also applied receiver operating characteristic (ROC) analysis and machine learning to identify potential diagnostic biomarkers. We offer openly accessible proteomic and metabolomic datasets that are readily available for researchers who lack access to clinical serum samples.

Methods

Study samples

In this study, a total of 16 healthy control individuals and 14 POF patients were recruited from the Reproductive Medicine Center of The Third Affiliated Hospital of Shenzhen University, China. Prior to analysis, serum samples were collected from all participants in

accordance with hospital standard operating procedures (SOPs). The inclusion of women with POF requires the presence of oligo/amenorrhea for at least 4 months in women below the age of 40, and with an increased follicle-stimulating hormone (FSH) serum concentration of >40 IU/L detected on at least two separate occasions>4 weeks apart. The exclude of healthy population is diagnosis of gynecological diseases with include criteria of normal menstrual period. For the cycle when the blood was drawn from patients, the POF patients' blood sample were collected three days after menstrual period if a POF patient has menstruation, and blood sample can be collected on any day if the POF patient has not menstruation, The patients were not under any medication. The blood hormone levels of luteinizing hormone (LH), follicle-stimulating hormone (FSH), and anti-Mullerian hormone (AMH) were subsequently tested using standardized assays. The POF patients were identified on the basis of their distinct blood hormone levels relative to those of the healthy control group. Serum was isolated from the collected blood samples by centrifugation at 3,000 rpm for 10 min and used for further extracellular vesicle extraction. These procedures were conducted to ensure the integrity and quality of the serum samples and to minimize any potential sources of experimental variability.

Extracellular vesicle extraction from serum

Standard inclusion and exclusion criteria were performed on the samples of the participants with a total of 10 ml of serum collected from healthy control and POF patient groups. The collected serum was transferred to a 15 ml centrifuge tube and centrifuged at 3,000 g for 15 min to remove cells and debris. The collected supernatant was transferred to a fresh 15 ml centrifuge tube and centrifuged at 10,000 g for 15 min to remove apoptotic bodies, RNA and proteins. Finally, the supernatant was transferred to an ultracentrifuge tube and centrifuged at 100,000 g for 2 h. The supernatant was discarded, and the extracellular vesicle pellet was resuspended in 100–500 µl of PBS. The extracted extracellular vesicles were frozen at -80 °C for further inspection.

Nanopore tracking analysis (NTA)

The extracellular vesicles suspended in PBS were gradient diluted and analyzed using a NanoFCM N30E nanoparticle tracking flow cytometer (NanoFCM, UK). Standard samples were tested before analyzing the extracellular vesicles. The nanoparticle size distribution and concentration were obtained from the machine and further analyzed using Origin 2018 (OriginLab Corporation, USA).

Transmission electron microscopy (TEM)

The morphology and dimensions of the extracellular vesicles were identified using an HT7700 transmission electron microscope (Hitachi, Japan). For sample preparation, 10 µl of the extracellular vesicle solution suspended in PBS was loaded on a copper mesh and allowed to precipitate for 1 min. Subsequently, the excess liquid was removed using filter paper. Next, 10 µl of phosphotungstic acid was deposited onto the copper mesh and allowed to precipitate for 1 min, after which the excess liquid was again removed using filter paper. The sample was air-dried at room temperature for 5 min and imaged at a voltage of 100 kV.

Western blotting

The extracellular vesicle suspension underwent lysis by adding 50% volume of RIPA lysis buffer (). The extracellular vesicles were lysis on ice for 30 min. The protein concentration was determined using the bicinchoninic acid (BCA) method. Equal amounts of total protein were mixed with loading buffer and boiled for 10 min to ensure protein denaturation. The 12% Bis-Tris Western blot gels prepared using gel making kit (Servicebio, China) were run at 80 V, with the voltage increased to 120 V upon observation of protein samples entering the separation gel. Protein transfer to a polyvinylidene fluoride (PVDF) membrane was carried out at 30 mA for an appropriate duration. The membrane was then blocked using a 5% BSA solution at room temperature on a shaker for 2 h. Primary antibodies, including those against TSG101 (Proteintech, 1:500), CD81 (Proteintech, 1:500), CD63 (Proteintech, 1:500), CD9 (Proteintech, 1:250), and Alix (Proteintech, 1:1000), were prepared accordingly. The blot was incubated overnight on a shaker at 4 °C. The following day, the membrane was washed four times for five minutes each with TBST on a shaker. The corresponding secondary antibody, diluted to 1:10,000, was applied and incubated at room temperature on a shaker for 1 h. The PVDF membrane was washed four times for five minutes each with TBST. Chemiluminescence was detected using Pierce ECL (Yeasen).

Proteomics

For the identification of serum-extracted exosomal proteins, the samples were thawed, washed, and homogenized with a lysate solution. The mixture underwent low-temperature ultrasound for 30 min (2 cycles) and was then stored at -20 °C for 1 h. Protein extraction was performed by denaturing the lysate, determining the protein concentration using Bradford method, and filtering the supernatant through ultrafiltration. A 100 µg protein solution was incubated with 10 mM dithiothreitol (DTT) at 37 °C for 1.5-2 h to reduce the proteins. Then, 25 mM iodoacetamide (IAA) was added and incubated

in darkness for 45 min to 1 h for alkylation. The protein solution was digested with trypsin at a 50:1 protein-to-trypsin ratio at 37 °C overnight. Each reaction was quenched by adjusting the pH to below 3 with 10% trifluoroacetic acid (TFA), desalted using an MCX C18 column, and the peptides were dried in a centrifugal vacuum evaporator following the manufacturer's instructions.

LC–MS/MS analysis

Peptides were separated using an easylc-1000 high-performance liquid chromatograph coupled to an Orbitrap Q Exactive mass spectrometer and analyzed using the Xcalibur software platform. A reversed-phase analytical column was used for chromatographic separation, with peptides eluted using a gradient of 6–90% solvent B over a span of 240 min at a flow rate of 250 nL/min. The electrospray voltage was set at 2.3 kV, and a scan range of 300 to 1500 m/z was used for the Orbitrap mass analyzer at a resolution of R=70,000.

Proteomic data analysis

The MS/MS data files were searched using Proteome Discoverer and screened for spectrograms, isotopic label purity correction, and quantitative data integration using the Proteomics Tool Suite. QC was done by illustrating parent ion mass tolerance distribution, an indicator of mass spectrometer performance and quality assessment. A minimum of 1 peptide was required for protein identification (Supplementary Table S4). Peptide and protein error rates were maintained below 1%. Differentially expressed proteins were considered significant if they exhibited fold changes>1.5 (or <0.67) and a P *value*<0.05. Functional enrichment analyses were conducted using Gene Ontology (GO) and the DAVID 6.7 databases, with the differentially expressed proteins categorized into biological process, cellular component, and molecular function. Related pathways were identified using the KEGG database.

Metabolomic sample preparation

To prepare samples for metabolomics analysis, 200 μL of ddH2O was added, and the samples were vortexed for 60 s. Subsequently, 800 μL of a methanol/acetonitrile mixture (1:1, v/v) was added, and the mixture was vortexed for another 60 s. After centrifugation at 14,000 g/min for 20 min at 4 °C, the resulting supernatant was freeze-dried and stored at -80 °C. For LC/MS analysis, lyophilized samples were dissolved in a 100 μL solvent mixture of water/acetonitrile (1:1, v/v), vortexed for 60 s, and then centrifuged at 14,000 × g for 10 min at 4 °C. The resulting supernatants were collected for further analysis.

LC/MS analysis

LC analysis was conducted using a Vanquish UHPLC System (Thermo Fisher Scientific, USA). Chromatography was performed on an ACQUITY UPLC® HSS T3 column (150×2.1 mm, 1.8 μm particle size) (Waters, Milford, MA, USA), with the column temperature maintained at 40 °C. The flow rate and injection volume were set at 0.25 mL/min and 2 μL, respectively. For LC-ESI (+)-MS analysis, the mobile phases consisted of 0.1% formic acid in acetonitrile (v/v) (C) and 0.1% formic acid in water (v/v) (D). Separation was achieved using the following gradient: 0 ~ 1 min, 2% C; 1 ~ 9 min, 2%~50% C; 9 ~ 12 min, 50%~98% C; 12 ~ 13.5 min, 98% C; 13.5 ~ 14 min, 98%~2% C; and 14 ~ 20 min, 2% C. For LC−ESI−MS analysis, the analytes were analyzed with (A) acetonitrile and (B) ammonium formate (5 mM). Separation was conducted under the following gradient: 0 ~ 1 min, 2% A; 1 ~ 9 min, 2%~50% A; 9 ~ 12 min, 50%~98% A; 12 ~ 13.5 min, 98% A; 13.5 ~ 14 min, 98%~2% A; and 14 ~ 17 min, 2% A.

Mass spectrometric detection of metabolites was conducted using an Orbitrap Exploris 120 mass spectrometer (Thermo Fisher Scientific, USA) equipped with an electrospray ionization (ESI) source. QC runs were compared with sample results. To identify biomarkers, the relative standard deviation (RSD) of potential characteristic peaks in QC samples must not exceed 30%. Features not meeting this criterion were eliminated. Simultaneous MS1 and MS/MS (full MS-ddMS2 mode, data-dependent MS/MS) acquisition was employed. The operational parameters were set as follows: sheath gas pressure, 30 arb; auxiliary gas flow, 10 arb; spray voltage, 3.50 kV and −2.50 kV for ESI(+) and ESI(-), respectively; capillary temperature, 325 ℃; MS1 range, m/z 100–1000; MS1 resolving power, 60,000 FWHM; number of data-dependent scans per cycle, 4; MS/MS resolving power, 15,000 FWHM; normalized collision energy, 30%; and dynamic exclusion time, automatic.

Combined metabolomics and proteomics analysis

To integrate insights from metabolomics and proteomics, differentially expressed proteins and metabolites were mapped to pathways using the KEGG database. Enrichment analysis was conducted using R to combine KEGG annotation and enrichment results, providing a comprehensive understanding of affected biological processes, cellular components, and molecular functions.

Random forest machine learning

The random forest algorithm, which employs ensemble learning, integrates multiple decision trees. In this study, proteomic data were utilized in a random forest classifier. The model was trained using the 'RandomForest' R package with specified parameters, except for 'n_trees' (set to 500) and 'max_depth' (set to 10). After stratified 10-fold

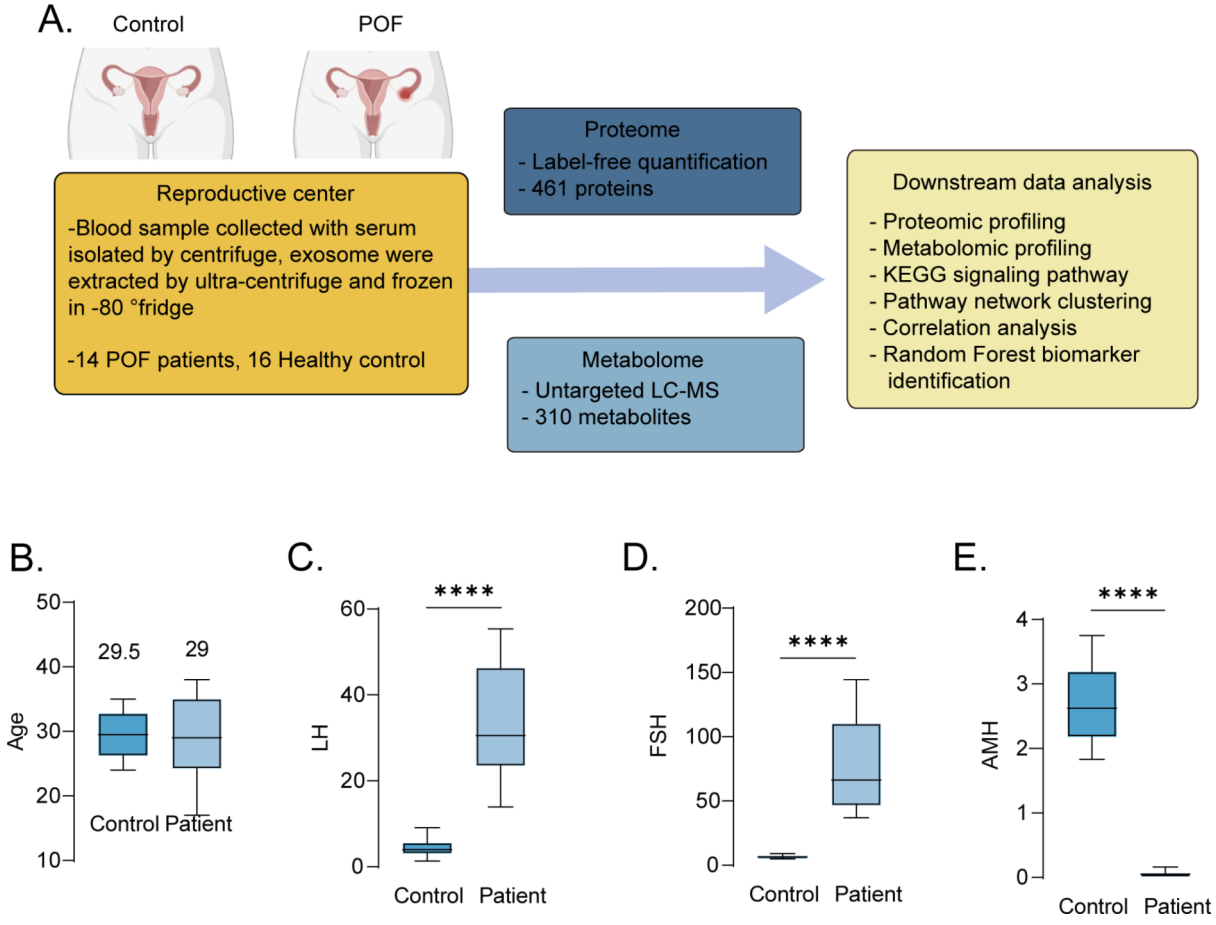

Fig. 1 Schematic summary **(A)** Schematic graph illustrating the sample collection, proteome and metabolome platforms and downstream analysis. **(B)** Age distribution of POF patients and healthy controls. **(C)** Blood LH distribution in POF patients and healthy controls. *P-value* < 0.001. **(D)** Blood FSH distribution in POF patients and healthy controls. *P-value* < 0.001. **(E)** Blood AMH distribution in POF patients and healthy controls. *P-value* < 0.001

Table 1 Characterization of study population

Characteristics	Healthy Control	POF patient	*P*-value
Mean (SD) age, year	29.38 ± 3.519	28.71 ± 7.097	0.7556
Menstruate cycle state	Regular	Irregular	
bFSH (IU/L)	6.51 ± 1.253	77.48 ± 35.973	< 0.0001
bLH (IU/L)	4.52 ± 2.013	33.43 ± 13.543	< 0.0001
bAMH (ng/ml)	2.71 ± 0.617	0.06 ± 0.036	< 0.0001

LH: luteinizing hormone, FSH: follicle-stimulating hormone, AMH: anti-Müllerian hormone

cross-validation, the importance ranking was illustrated based on importance values.

Statistical analyses

Statistical analyses were performed using GraphPad Prism version 8.3.0. Clinical data are presented as the mean ± standard deviation. Proteomic and metabolomic data were log2-transformed and median normalized. One-way ANOVA and unpaired t tests with Welch's correction were employed to evaluate statistical significance. A *P value* < 0.05 was considered significant.

Results

Characterization of patient population and extracted extracellular vesicles

The current investigation enrolled a cohort of 30 participants, comprising 16 healthy controls and 14 patients diagnosed with POF, sourced from the Reproductive Medicine Center of the Third Affiliated Hospital of Shenzhen University, China (Fig. 1A). The clinical characteristics of the subjects are concisely presented in Table 1. The age distributions within both the patient and control groups were similar (Fig. 1B). Nevertheless, comparative analysis revealed irregular menstrual cycles among POF patients in contrast to healthy controls. Moreover, discernible elevations in the levels of luteinizing hormone (LH) and follicle-stimulating hormone (FSH) were observed in the peripheral blood of POF patients (Fig. 1C & D), accompanied by a notable reduction in anti-Müllerian hormone (AMH) levels (Fig. 1E), indicating decreased ovarian function in POF patients relative to healthy controls.

The extracellular vesicles derived from both cohorts exhibited similar characteristics. Particle size analysis was conducted to determine the average diameter of the extracellular vesicles, revealing a diameter of 90.02 nm (Figure S1A). Subsequent examination of the morphological features of the extracellular vesicles via transmission electron microscopy revealed the presence of double-membrane pitted vesicles with a saucer-like configuration, consistent with previously documented exosomal structures (Figure S1B). Additionally, to validate the extraction of extracellular vesicles, Western blotting analysis was performed to identify extracellular vesicle-specific protein markers, including CD9, CD63, CD81, Alix, and TSG101 (Figure S1C).

Proteomic profiles identifying pre- and Pro-POF patient subgroups

In this investigation, a quantitative proteomic analysis of serum-extracted extracellular vesicles was conducted utilizing label-free mass spectrometry to construct the proteomic profile of POF patients. Initially, principal component analysis (PCA) was employed to categorize the patients and healthy volunteers. The results revealed that the patient group could be subdivided into two distinct subgroups: Pre and Pro (Fig. 2A). The subgroup designated Pre exhibited similarities with the healthy controls, whereas the subgroup designated Pro clearly distinguished itself from the healthy controls.

The differentially expressed proteins within the patient subgroups compared to the healthy cohort are illustrated using volcano plots, highlighting proteins with a fold change > 2 and a *P value* < 0.05, with the top ten proteins highlighted (Fig. 2B & C). Approximately 58 differentially

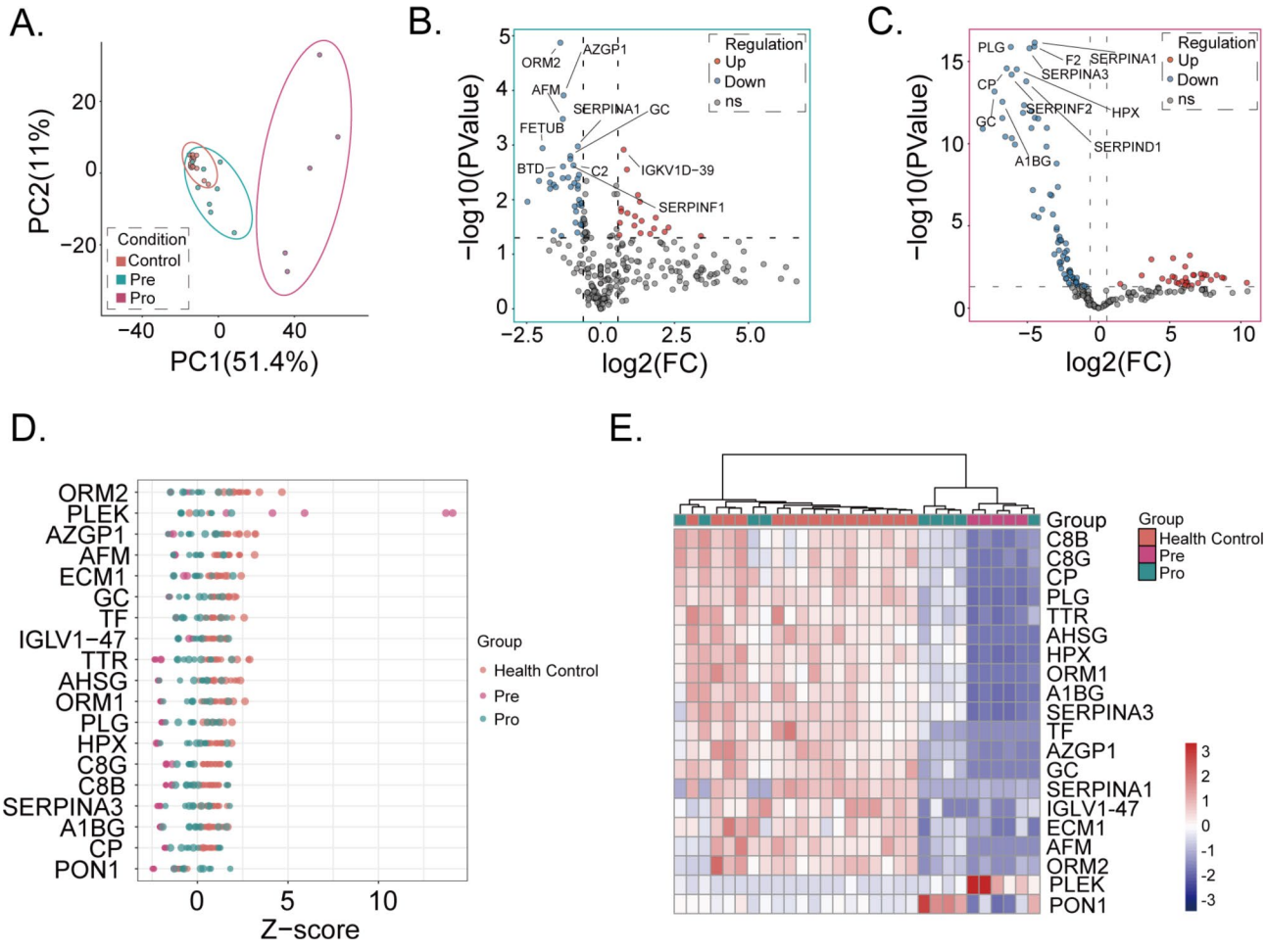

Fig. 2 Exosomal proteomic analysis of differentially expressed proteins among POF patients and healthy controls. **(A)** PCA plot of proteomic data from POF patients and healthy controls. Subgroups of POF patients were selected and named Pre and Pro. **(B)** Volcano plot of Pre-POF and healthy control proteins. The top 10 differentially expressed proteins are annotated in the graph. **(C)** Volcano plot of Pro-POF and healthy control proteins. The top 10 differentially expressed proteins are annotated in the graph. **(D)** Z score graph of differentially expressed proteins in the Pre-POF, Pro-POF, and healthy control groups. **(E)** Multigroup heatmap cluster of differentially expressed proteins in the Pre-POF, Pro-POF, and healthy control groups

expressed proteins were detected between Pre-POFs and healthy controls (Fig. 2B). However, 105 differentially expressed proteins were identified between the Pro-POF group and the healthy control group, consistent with our PCA findings indicating that the Pro-POF group was more distinctly separated from the healthy control group (Fig. 2C). Among the top DEPs in Pre-POF patients compared to healthy controls, ORM2 was the most significantly decreased (FC=0.389, $P=1.336\times10^{-5}$), and the SERPIN family members SERPINA1 (FC=0.587, $P=1.057\times10^{-3}$) and SERPINF1 (FC=0.492, $P=1.806\times10^{-3}$) were also significantly decreased (Supplementary table S1). Among the top DEPs in the Pro-POF group compared to the healthy control group, the most significantly decreased were the SERPINA1 (FC=0.044, $P=7.077\times10^{-17}$), SERPINA3 (FC=0.035, $P=1.569\times10^{-16}$), SERPINF2 (FC=0.014, $P=6.27\times10^{-15}$), and SERPIND1 (FC=0.030, $P=1.623\times10^{-13}$) families (Supplementary table S2).

To further elucidate the differences among the three groups, a Z score graph was generated to represent protein expression in each sample, revealing the 19 proteins differentially expressed between Pre and Pro POF (Fig. 2D). Additionally, proteomic data analysis of the entire cohort of POF patients and healthy controls revealed 69 differentially expressed proteins (Figure S2A). However, heatmap clustering indicated that these identified differentially expressed proteins could not effectively discriminate between the three groups (Figure S2B). Nevertheless, heatmap clustering revealed that the 19 proteins could distinguish healthy controls from both POF subgroups (Fig. 2E).

Metabolomic profiling distinguishes patient and healthy cohorts

We subsequently conducted a metabolomic analysis employing LC/MS to discern the disparities in metabolite profiles between the patients and healthy controls. Principal component analysis (PCA) revealed similarities between the two groups (Fig. 3A). Due to the intricate nature of the metabolomic dataset, partial least squares discriminant analysis (PLS-DA) was employed to segregate samples from the two groups, revealing clear differentiation without identifiable subgroups (Fig. 3B).

The differentially expressed metabolites were identified and are illustrated by a volcano plot, which highlights the top 10 disparities (Fig. 3C). Among the 31 DEMs, norselegiline (FC=0.54, $P=1.06\times10^{-7}$) appeared to be the most significantly decreased metabolite (Supplementary table S3). Z score analysis of the differentially expressed metabolites revealed high variability within the healthy controls (Fig. 3D). Most identified metabolites exhibited lower expression levels in the patient group, with only L-phenylalanine, 3-hydroxyanthranilate, 2-doxystreptamine, uracil 5-carboxylate, and phosphoenolpyruvic acid showing upregulation. Furthermore, we utilized the differentially expressed metabolites to generate a heatmap, which clearly distinguished between the two groups (Fig. 3E).

Pathway network clustering reveals progressive metabolic dysfunction in POF patients

To elucidate the molecular mechanisms underlying the pathogenesis of POF, we initially conducted a KEGG analysis of proteomic and metabolomic data. Proteomic results revealed significant upregulation of the Rap1 signaling pathway and the peroxisome proliferator-activated receptor (PPAR) signaling pathway in POF patients (Figure S3A). Concurrently, metabolomic analysis indicated a significant alteration in tyrosine synthesis and metabolism (Figure S3B). To further discover the signaling pathways contributing to the development of POF, we integrated the KEGG datasets and revealed 5 pathways shared between the Pre-POF group and the healthy control group (Fig. 4A). In contrast, 14 common pathways were identified between the Pro-POF group and the healthy control group, with only the mineral absorption and metabolic pathways being shared between them (Fig. 4B). The Pro-POF group exhibited significant downregulation of glycolysis, pyruvate metabolism, and the glucagon signaling pathway compared to the Pre-POF group, indicating a progressive dysfunction of energy metabolism.

Norselegiline and transthyretin (TTR) were identified as pivotal nodes in the two primary clusters of proteomic and metabolomic pathway network clustering between Pre-POF patients and healthy controls (Fig. 4C). Norselegiline exhibited a positive correlation with the serpin family, while TTR displayed a positive association with L-phenylalanine, which is responsible for tyrosine synthesis. Furthermore, comparison of Pro-POF to Pre-POF revealed a greater degree of association between proteins and metabolites, with norselegiline remaining a central node in the network, along with gentisic acid, vanillylmandelic acid, cellobiose, dimethylglycine, (+)-cis-isopulegone, and 2-oxoarginine, all of which are suggested to play essential roles in the network (Fig. 4D).

DEPs were found to be strongly associated with DEMs

POF patients were divided into two distinct subgroups according to the progression of dysfunctional metabolic signaling pathways. The subsequent objective was to discover potential biomarkers of this disease that could predict the onset of POF. Correlation heatmap clustering revealed that the DEPs and DEMs were either significantly positively or negatively correlated (Fig. 5A). To investigate whether consistent proteins or metabolites exist that could distinguish POF patients from healthy

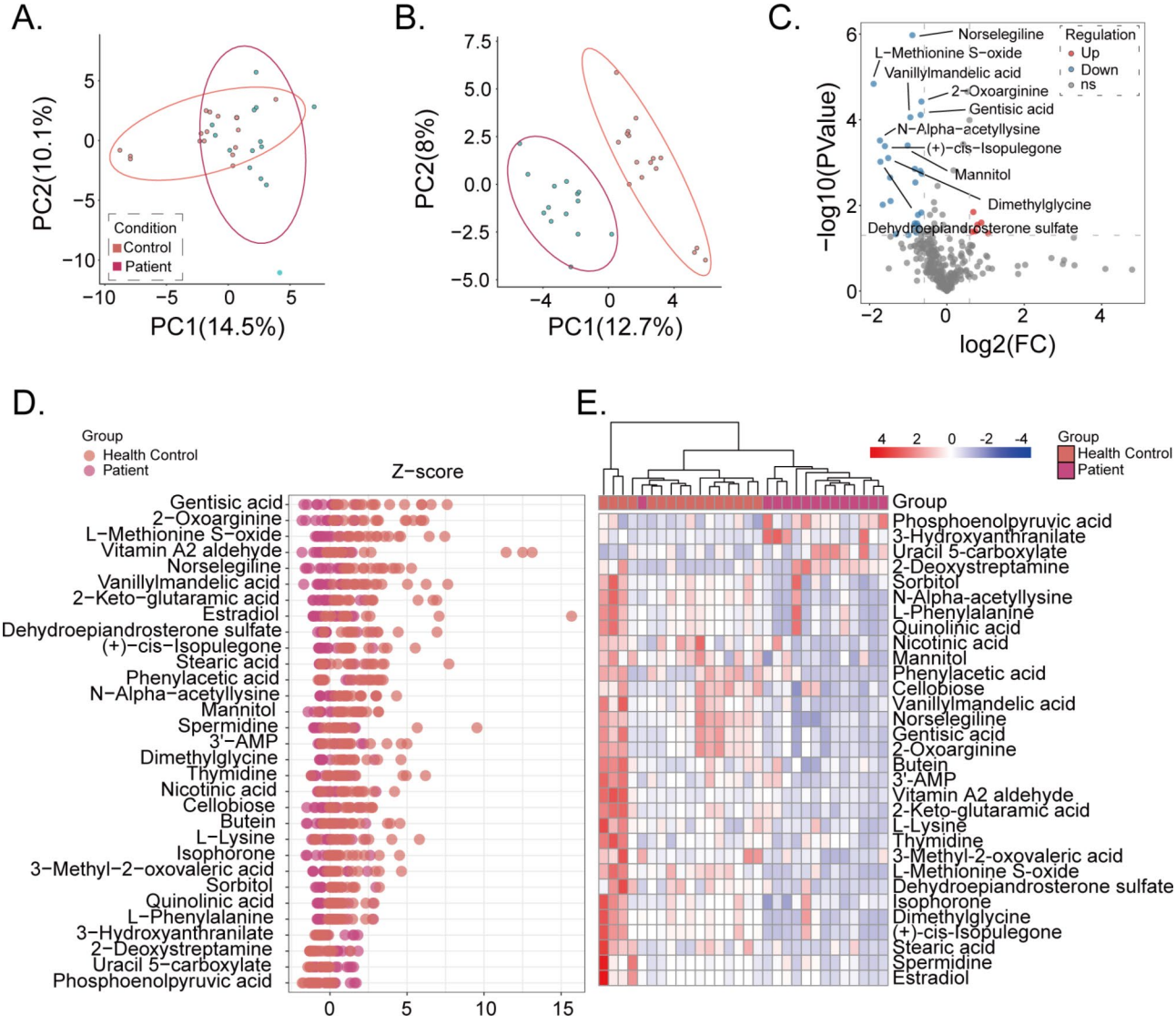

Fig. 3 Exosomal metabolomic analysis of differentially expressed metabolites among POF patients and healthy controls. **(A)** PCA plot of proteomic data from POF patients and healthy controls. Subgroups of POF patients were selected and named Pre and Pro. **(B)** PLS-DA plot of proteomic data from POF patients and healthy controls. Subgroups of POF patients were selected and named Pre and Pro. **(C)** Volcano plot of POF patient and healthy control metabolites. The top 10 differentially expressed metabolites are annotated in the graph. **(D)** Z score graph of differentially expressed proteins in POF patients and healthy controls. **(E)** Heatmap cluster of differentially expressed metabolites between POF patients and healthy controls

controls, we constructed a Sankey diagram highlighting the most correlated proteins and metabolites among the groups. The results indicated that three clusters of metabolites were positively regulated by six protein clusters but negatively regulated by CFH, FGG, and SERPINF1 (Fig. 5B). In contrast to the Pre-POF group, the Pro-POF group exhibited only two clusters of metabolites that were positively regulated by nine protein clusters but negatively regulated by PFN1, ACTN1, and IGHV3-64D (Fig. 5C). This indicates that there exist protein and metabolite correlation during the progression of POF. The remaining correlation during the progression of the disease must be consistent and holds the potential to be applied as biomarkers.Two proteins and four metabolites appeared in both analyses and were selected as the initial pool to identify potential biomarkers.

Identification of POF biomarkers

The fold changes of the previously identified proteins and metabolites were initially computed. The relative expression levels of these molecules in the two groups are shown, all of which exhibited significantly low expression levels in POF patients (Fig. 6A). Notably, quinolinic acid and L-phenylalanine displayed high variation among POF patients, suggesting their potential inadequacy as predictive biomarkers. Subsequent ROC analysis involving

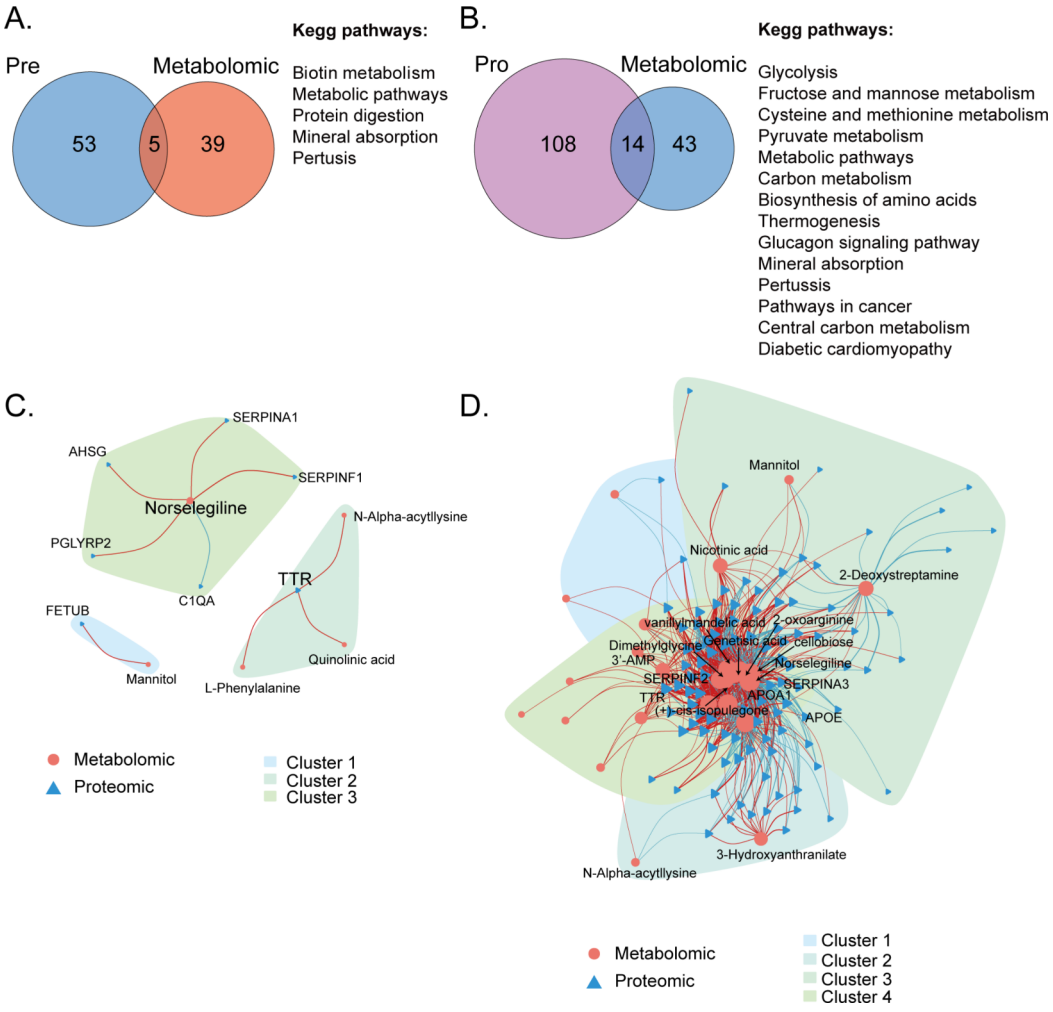

Fig. 4 Signaling pathway network clustering **(A)** Venn diagram illustrating the number of signaling pathways significantly changed in Pre-POF patients and healthy controls. Each signaling pathway analysis was conducted based on the identified differentially expressed proteins or metabolites, and the results are shown in orange (protein) and blue (metabolite) in the graph. **(B)** Venn diagram illustrating the number of signaling pathways significantly changed in Pro-POF patients and healthy controls. Each signaling pathway analysis was conducted based on the identified differentially expressed proteins or metabolites, and the results are shown in purple (protein) and blue (metabolite) in the graph. **(C)** Network clustering of identified signaling pathways between Pre-POF patients and healthy controls. Metabolites (circles) and proteins (triangles) were labeled with connecting lines to indicate their regulatory roles: red (positive) and blue (negative). **(D)** Network clustering of identified signaling pathways between Pro-POF patients and healthy controls. Metabolites (circles) and proteins (triangles) were labeled with connecting lines to indicate their regulatory roles: red (positive) and blue (negative). Significant nodes in the clusters were annotated. Source data are provided in the source data file

quinolinic acid and L-phenylalanine yielded lower AUC values, consistent with their expression patterns in the two groups (Fig. 6B).

We subsequently employed random forest machine learning to assess the significance of each selected factor in distinguishing POF patients from healthy controls. The results indicated that AFM was the most crucial factor, while quinolinic acid and L-phenylalanine were the least significant factors (Fig. 6C). However, decision tree model testing revealed that although the AFM was suggested to be the most important parameter for predicting the occurrence of POF, it alone could not accurately discriminate between the two groups, as illustrated by an accuracy rate of 10 out of 21 in the decision tree structure (Fig. 6D). Among the remaining metabolites, gentisic acid were generally considered as exogenous metabolite to be excluded (Supplementary table S5). In combination with 2-oxoarginine, the accuracy rate was the highest and reaching 95.2%, suggesting that AFM in conjunction with 2-oxoarginine could serve as a biomarker for precise diagnosis of POF.

Discussion

In our omic analysis of the protein and metabolite contents within serum-extracted extracellular vesicles, we identified key disease pathways contributing to the development of POF and identified potential biomarkers for predicting its occurrence. Overall pathway analysis of the

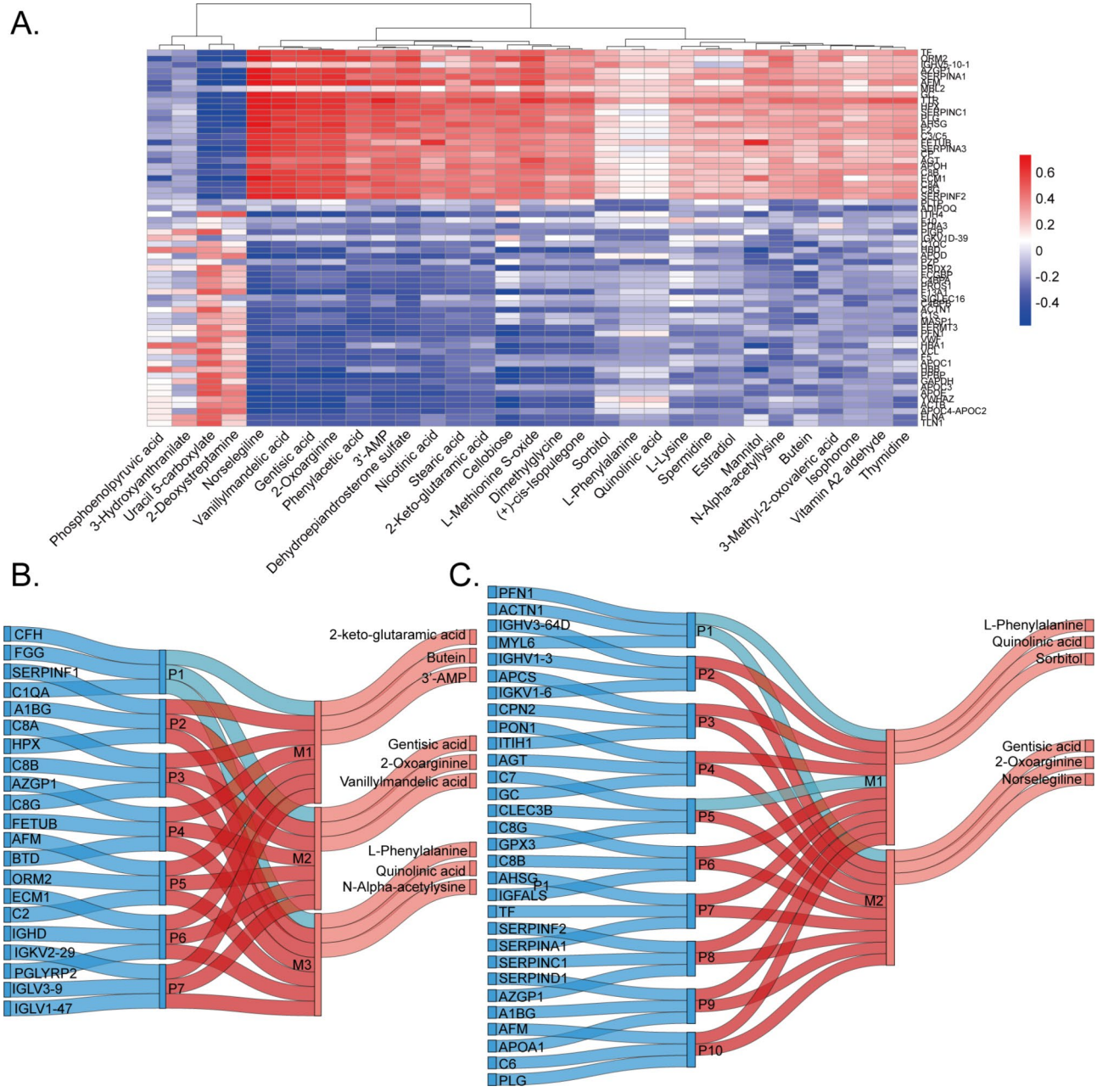

Fig. 5 Correlation analysis of the proteome and metabolome **(A)** Correlation heatmap of differentially expressed proteins and metabolites in POF patients. Red represents a positive correlation. Blue represents a negative correlation. **(B)** Sankey diagram of differentially expressed proteins and metabolites in Pre-POF patients and healthy controls. The top three genes in each cluster were annotated. In the middle, red represents a positive correlation, and blue represents a negative correlation. **(C)** Sankey diagram of differentially expressed proteins and metabolites in Pro-POF patients and healthy controls. The top three genes in each cluster were annotated. In the middle, red represents a positive correlation, and blue represents a negative correlation

protein profile suggested abnormalities in the Rap1 and PPAR signaling pathways in POF patients. Rap1, a close relative of the GTPase Ras, is activated by extracellular signals and contributes to various biological processes, including cell growth, differentiation, adhesion, and morphogenesis [19]. Mesenchymal stem cells (MSCs) have shown significant therapeutic effects on ovarian function recovery and are suggested as a potential treatment for POF [20]. The therapeutic function of MSCs may result from their paracrine function, which is regulated by the Rap1/NFκB signaling pathway [21]. Furthermore, recent studies have indicated that treatment with ZSYTP improves ovarian function in a POI model, and RNA-seq results revealed that the Rap1 signaling pathway is a potential treatment mechanism [22]. These findings suggest that negative regulation of Rap1 might lead to

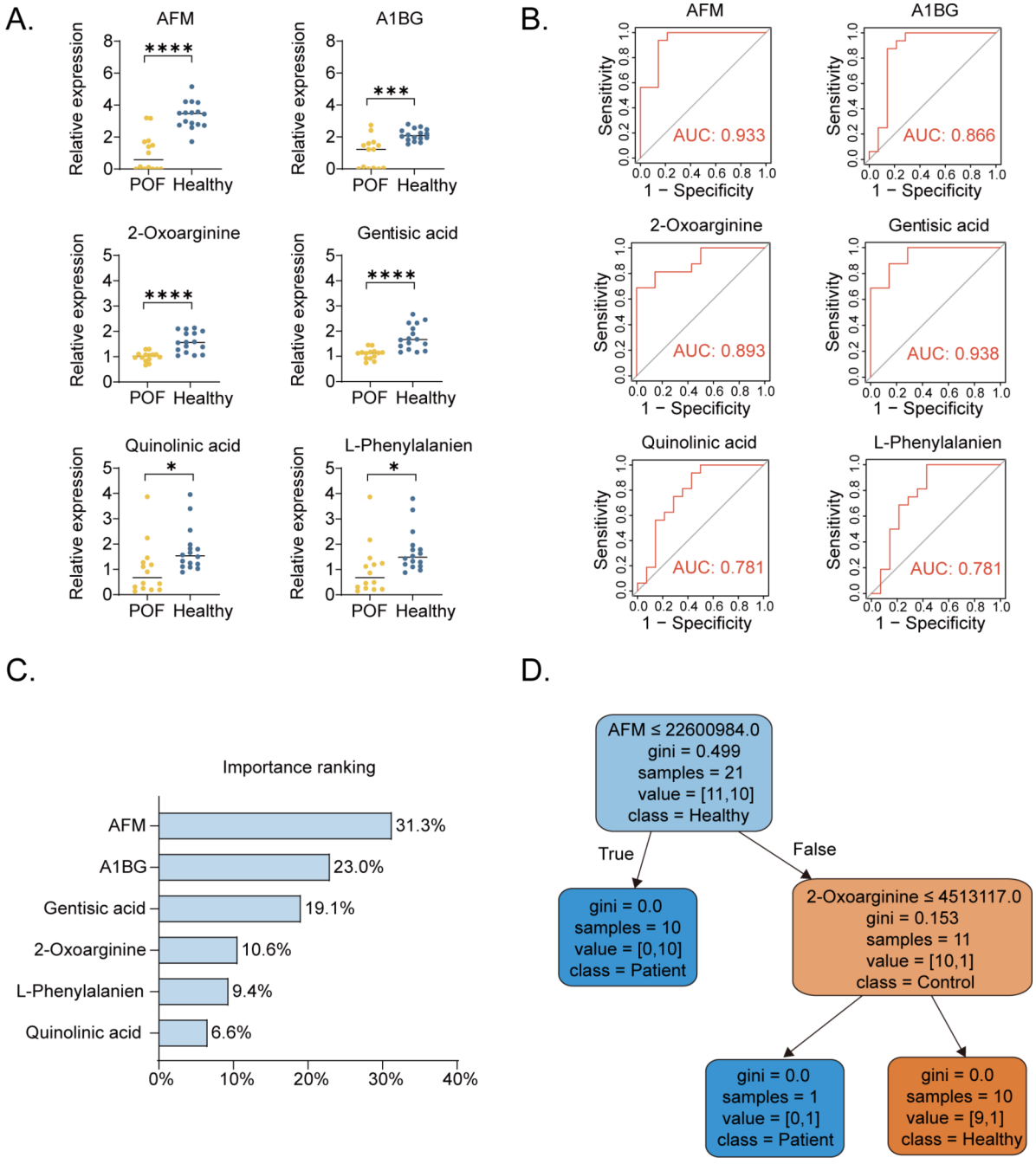

Fig. 6 Identification of diagnostic biomarkers **(A)** Expression of selected proteins and metabolites. P values were calculated and are presented as (* < 0.05, ****<0.0001). **(B)** ROC curve of selected proteins and metabolites. The area under the curve (AUC) was calculated and is illustrated in the graph. **(C)** Importance ranking of selected proteins and metabolites. The importance score was calculated by random forest machine learning. **(D)** Decision tree model constructed by applying AFM and 2-oxoarginine as POF diagnostic biomarkers. Twenty-one samples were chosen for diagnosis. The accuracy of the decision model is 95.2% (20/21)

inflammation, thereby contributing to the development of POF. Additionally, recent studies have suggested that CXCl10 is a diagnostic biomarker of POF, with enrichment analysis indicating activation of the PPAR signaling pathway in POF patients [23]. Metformin has been found to alleviate chemotherapy-induced POF by protecting granulosa cells [24]. Database analysis and Western blot verification suggested that metformin alleviates M1 macrophage-induced GC injury through the downregulation of PPARγ, implicating the PPAR signaling pathway in inflammation and the development of POF.

Moreover, PCA of the proteomic profile suggested the existence of subgroups within the POF patient cohort. In pre-POF patients, FETUB encodes the fetuin B protein, which is necessary for maintaining zona pellucida (ZP) permeability [25]. Deficiency in pre-POF patients suggests difficulties in fertility. Among the Pre- and Pro-POF subgroups, the SERPIN superfamily was among the most downregulated proteins. Although the commonly identified SERPINA1 gene has not been previously reported in POF patients, its encoded protein, alpha-1-antitrypsin (AAT), functions to protect tissues during inflammation [26]. Thus, the proteomic profile suggested that early signaling affects fertility in POF patients, with inflammation potentially damaging ovarian tissues.

Metabolomic profiling revealed the downregulation of most metabolites in POF patients, with norselegiline being the most significant. Norselegiline, a specific metabolite of selegiline, is involved in the rapid metabolism of selegiline, a monoamine oxidase inhibitor used in Parkinson's disease treatment [27]. Despite its therapeutic effects, selegiline has been suggested to attenuate oxidative stress and apoptosis in a cardiac disease rabbit model by downregulating Bcl-2 and Bax expression [28]. Signaling pathway analysis suggested alterations in ABC transporters, protein digestion and absorption, and central carbon metabolism, consistent with previous metabolomic findings [28]. Additionally, downregulation of the estrogen signaling pathway and endocrine reabsorption reflects hormone imbalances commonly observed in POF patients.

Correlation pathway analysis revealed alterations in mineral absorption and metabolic pathways in two subgroups of POF patients. Mineral absorption is strongly associated with previously identified ABC transporters, which play a role in translocating metal ions [29]. Glycolysis, pyruvate metabolism, and the glucagon signaling pathway were significantly affected in the pro-POF subgroup, suggesting progressive dysfunction of energy metabolism during disease development. Node network clustering identified key proteins and metabolites contributing to changes in signaling pathways. Norselegiline remained the most important node in both groups, while FETUB was severely downregulated in the pre-POF group, suggesting positive regulation by mannitol. Transthyretin (TTR) has been identified as a metabolite that functions as a transporter of thyroid hormone into the brain, with highly activated thyroid hormone being associated with poor ovarian function reserve [30–32]. In the pro-POF subgroup, gentisic acid, cellobiose, dimethylglycine, and (+)-cis-isopulegone were important nodes. Gentisic acid reportedly alleviates type 2 diabetes by modulating inflammatory pathways in macrophages [33, 34]. Cellobiose plays a role in energy metabolism [35], dimethylglycine is an amino acid used to improve energy and boost the immune system [36–38], and (+)-cis-isopulegone reflects energy metabolism [39]. This evidence agrees with previous findings that dysfunction of energy metabolism occurs in POF patients, while other factors, such as inflammation and hormone imbalance, contribute to the development of this disease.

Furthermore, our research narrowed the population of DEPs and DEMs through regulatory clustering, suggesting that AFM, A1BG, 2-oxoarginine, gentisic acid, quinolinic acid, and L-phenylalanine are consistent biomarkers for POF patients. Random forest machine learning revealed that AFM combined with gentisic acid can accurately predict the occurrence of POF. AFM encodes the Afamin protein, which facilitates vitamin E transport across the blood–brain barrier and has been reported to be a promising biomarker for POI diagnosis [40–42]. However, studies have reported it is a potential biomarker for several diseases, making it insufficient as a POF biomarker [43, 44]. 2-Oxoarginine has been detected in metabolome profiles of disease models of cerebral ischemia/reperfusion mice and rheumatoid arthritis rats [45, 46]. However, no evidence suggests its relationship with ovarian functions. 2-Oxoarginine was known for its role in the urea cycle as a metabolite of arginine catabolism. Study has found that impaired arginine metabolism is associated with poor ovarian function in Polycystic Ovary Syndrome. The lower expression of 2-oxoarginine in my study could signal ovarian dysfunction of POF patients [47]. Therefore, the abnormal expression of both AFM and 2-oxoarginine together serves as a diagnostic biomarker for POF.

However, this study was limited by the low number of samples analyzed. Due to individual complexities, a smaller clinical sample might not be sufficient to comprehensively reveal the commonalities identified in each group. Consequently, the results may be biased, necessitating further research with an expanded clinical sample to verify the findings.

This study is the first to apply omic analysis of proteomic and metabolomic profiles to clinical serum-extracted extracellular vesicles from POF patients compared to those from healthy controls. The proteomic profile indicates the division of POF patients into two subgroups based on exosomal protein content, with both subgroups sharing pathological pathways contributing to inflammation activation, and causing ovarian function damage. Metabolomic analysis revealed enhanced oxidative stress, apoptosis, and hormone imbalance in POF patients. Our study provides novel findings for identifying the progression of energy metabolism dysfunction during POF development through omic pathway network analysis. We reported the novel identification of AFM combined with 2-oxoarginine as a diagnostic biomarker for POF patients through further machine learning

analysis. In addition to providing an exosomal proteomic and metabolomic database, our pathway analysis and biomarker identification have novel diagnostic and therapeutic implications.

Abbreviations

AAT	Alpha-1-Antitrypsin
ABC	ATP-Binding Cassette
AFM	Afamin
AMH	Anti-Mullerian Hormone
BCA	Bicinchoninic Acid
DEPs	Differentially Expressed Proteins
DEMs	Differentially Expressed Metabolites
ESI	Electrospray Ionization
EVs	Extracellular vesicles
FGG	Fibrinogen Gamma Chain
FSH	Follicle-Stimulating Hormone
GO	Gene Ontologylsobaric
Itraq	Tags for Relative and Absolute Quantification
KEGG	Kyoto Encyclopedia of Genes and Genomes
LC	Liquid Chromatography
LC/MS	Liquid Chromatography/Mass Spectrometry
LH	Luteinizing Hormone
MS	Mass Spectrometry
MS/MS	Tandem Mass Spectrometry
MSCs	Mesenchymal Stem Cells
NFκB	Nuclear Factor Kappa B
NTA	Nanopore Tracking Analysis
PCA	Principal Component Analysis
PLS-DA	Partial Least Squares Discriminant Analysis
POF	Premature Ovarian Failure
ROC	Receiver Operating Characteristic
TTR	Transthyretin
TEAB	Triethylammonium Bicarbonate
TEM	Transmission Electron Microscopy
UHPLC	Ultra-High Performance Liquid Chromatography
ZP	Zona Pellucida

Supplementary Information

The online version contains supplementary material available at https://doi.org/10.1186/s12958-024-01277-9.

Supplementary Material 1: Characterization of serum-extracted extracellular vesicles. A Nanoparticle tracking analysis (NTA) showing the size distribution of isolated extracellular vesicles. Each particle's diameter along with the corresponding number of events is annotated. The mean diameter of the particles is 90.02 nm. B Transmission electron microscopy (TEM) images depicting the morphology of the extracellular vesicles. C Western blot analysis of exosomal protein markers including CD9, CD63, CD81, Alix, and TSG101. Molecular weights (kDa) are labeled on the right

Supplementary Material 2: Proteomic profile of identified DEPs between POF patient and Healthy control. A Volcano plot of POF patient and healthy control proteins. B Heatmap cluster of differentially expressed proteins in POF patients and healthy controls

Supplementary Material 3: KEGG analysis of Proteomic and metabolomic profiles. A KEGG analysis of differentially expressed proteins between POF patients and healthy controls. Number of proteins participate in the signaling pathway was illustrated by Prot. Number. B KEGG analysis of differentially expressed metabolites between POF patietns and healthy controls. Pathway size refers to the number of metabolites participate in the signaling pathway

Supplementary Material 4

Supplementary Material 5

Supplementary Material 6

Supplementary Material 7

Supplementary Material 8

Supplementary Material 9

Supplementary Material 10

Acknowledgements
Not applicable.

Author contributions
Zhen Liu: conception and design of the study, acquisition of samples for analysis, interpretation of data, and drafting of the article. Qilin Zhou: acquisition of samples for analysis, interpretation of data, revision of the article; Liangge He: interpretation of data, revision of the article; Zhengdong Liao, Yajing Cha, Hongyu Zhao, and Wenchao Zheng: acquisition of samples for analysis; Desheng Lu, revision of the article; Sheng Yang: conception and design of the study, funding of the study, acquisition of samples for analysis, interpretation of the data, drafting of the article and final approval for submission.

Funding
This study was supported by research grants from the Natural Science Foundation of Guangdong Province (2021A1515011132), Shenzhen Fundamental Research Program (JCYJ20190808122003692) and Shenzhen Science and Technology Program (JCYJ202208183000389).

Data availability
The authors have made all data pertinent to this study publicly accessible. The mass spectrometry metabolomics data are available at the Metabolomics Workbench under DataTrack ID 4782. Similarly, the mass spectrometry proteomics data can be found at the ProteomeXchange Consortium through the PRIDE partner repository, using dataset identifier PXD051569. Additionally, the source data for all figures and tables presented are included in a Source Data file. The generated analysis data from this study are available in the published article and the supplementary files.

Declarations

Ethics approval and consent to participate
For the human study, we obtained written informed consent from all participants. The study received approval from the Research Ethics Committee of the Third Affiliated Hospital of Shenzhen University, Shenzhen, China, under the authorization protocol number 2021-LHRMYY-SZLL-011. This study was conducted in accordance with the principles outlined in the Declaration of Helsinki.

Consent for publication
Not applicable.

Competing interests
The authors declare no competing interests.

Author details
[1]Guangdong Key Laboratory for Biomedical Measurements and Ultrasound Imaging, School of Biomedical Engineering, National-Regional Key Technology Engineering Laboratory for Medical Ultrasound, Shenzhen University Medical School, Shenzhen, China
[2]The Reproductive Medicine Center, The Third Affiliated Hospital of Shenzhen University, No. 47 Youyi Rd, Shenzhen, China
[3]Shenzhen University Medical School, Shenzhen, China
[4]Guangdong Provincial Key Laboratory of Regional Immunity and Diseases, Department of Pharmacology, Carson International Cancer Center, Shenzhen University Medical School, Shenzhen, China

Received: 4 June 2024 / Accepted: 5 August 2024
Published online: 19 August 2024

References

1. Jankowska K. Premature ovarian failure. Przeglad Menopauzalny = Menopause Rev. 2017;16(2):51–6.
2. Kovanci E, Schutt AK. Premature ovarian failure: clinical presentation and treatment. Obstet Gynecol Clin N Am. 2015;42(1):153–61.
3. Armeni E, Paschou SA, Goulis DG, Lambrinoudaki I. Hormone therapy regimens for managing the menopause and premature ovarian insufficiency. Best Pract Res Clin Endocrinol Metab. 2021;35(6):101561.
4. Yang Y, Huang W, Yuan L. Effects of Environment and Lifestyle factors on premature ovarian failure. Adv Exp Med Biol. 2021;1300:63–111.
5. Grossmann B, Saur S, Rall K, Pecher AC, Hubner S, Henes J, Henes M. Prevalence of autoimmune disease in women with premature ovarian failure. Eur J Contracept Reproductive Health care: Official J Eur Soc Contracept. 2020;25(1):72–5.
6. Slopien R, Warenik-Szymankiewicz A. Premature ovarian failure: diagnosis and treatment. Clin Exp Obstet Gynecol. 2014;41(6):659–61.
7. Montano KJ, Loukas A, Sotillo J. Proteomic approaches to drive advances in helminth extracellular vesicle research. Mol Immunol. 2021;131:1–5.
8. Johnson CH, Ivanisevic J, Siuzdak G. Metabolomics: beyond biomarkers and towards mechanisms. Nat Rev Mol Cell Biol. 2016;17(7):451–9.
9. Bai B, Wang X, Li Y, Chen PC, Yu K, Dey KK, Yarbro JM, Han X, Lutz BM, Rao S, et al. Deep Multilayer Brain Proteomics identifies Molecular Networks in Alzheimer's Disease Progression. Neuron. 2020;105(6):975–e991977.
10. Horgusluoglu E, Neff R, Song WM, Wang M, Wang Q, Arnold M, Krumsiek J, Galindo-Prieto B, Ming C, Nho K, et al. Integrative metabolomics-genomics approach reveals key metabolic pathways and regulators of Alzheimer's disease. Alzheimer's Dement J Alzheimer's Assoc. 2022;18(6):1260–78.
11. Joshi A, Rienks M, Theofilatos K, Mayr M. Systems biology in cardiovascular disease: a multiomics approach. Nat Reviews Cardiol. 2021;18(5):313–30.
12. Wang LB, Karpova A, Gritsenko MA, Kyle JE, Cao S, Li Y, Rykunov D, Colaprico A, Rothstein JH, Hong R, et al. Proteogenomic and metabolomic characterization of human glioblastoma. Cancer Cell. 2021;39(4):509–e528520.
13. Lee DH, Pei CZ, Song JY, Lee KJ, Yun BS, Kwack KB, Lee EI, Baek KH. Identification of serum biomarkers for premature ovarian failure. Biochim et Biophys acta Proteins Proteom. 2019;1867(3):219–26.
14. Chen J, Zhou Q, Zhang Y, Tan W, Gao H, Zhou L, Xiao S, Gao J, Li J, Zhu Z. Discovery of novel serum metabolic biomarkers in patients with polycystic ovarian syndrome and premature ovarian failure. Bioengineered. 2021;12(1):8778–92.
15. Yotsukura S, Mamitsuka H. Evaluation of serum-based cancer biomarkers: a brief review from a clinical and computational viewpoint. Crit Rev Oncol/Hematol. 2015;93(2):103–15.
16. Cocucci E, Meldolesi J. Ectosomes and extracellular vesicles: shedding the confusion between extracellular vesicles. Trends Cell Biol. 2015;25(6):364–72.
17. Jiang X, Li J, Zhang B, Hu J, Ma J, Cui L, Chen ZJ. Differential expression profile of plasma exosomal microRNAs in women with polycystic ovary syndrome. Fertil Steril. 2021;115(3):782–92.
18. Zhang L, Li H, Yuan M, Li D, Sun C, Wang G. Serum Exosomal MicroRNAs as Potential Circulating Biomarkers for Endometriosis. *Disease markers* 2020, 2020:2456340.
19. Bos JL, de Rooij J, Reedquist KA. Rap1 signalling: adhering to new models. Nat Rev Mol Cell Biol. 2001;2(5):369–77.
20. Shareghi-Oskoue O, Aghebati-Maleki L, Yousefi M. Transplantation of human umbilical cord mesenchymal stem cells to treat premature ovarian failure. Stem Cell Res Ther. 2021;12(1):454.
21. Zhang Y, Chiu S, Liang X, Gao F, Zhang Z, Liao S, Liang Y, Chai YH, Low DJ, Tse HF, et al. Rap1-mediated nuclear factor-kappab (NF-kappaB) activity regulates the paracrine capacity of mesenchymal stem cells in heart repair following infarction. Cell Death Discovery. 2015;1:15007.
22. Song Z, Song K, Zhao H, He Y, Hu J. Network analysis and experimental approach to investigate the potential therapeutic mechanism of zishen yutai pills on premature ovarian insufficiency. Heliyon. 2023;9(9):e20025.
23. Qin Y, Wen C, Wu H. CXCL10-based gene cluster model serves as a potential diagnostic biomarker for premature ovarian failure. PeerJ. 2023;11:e16659.
24. Yang Y, Tang X, Yao T, Zhang Y, Zhong Y, Wu S, Wang Y, Pan Z. Metformin protects ovarian granulosa cells in chemotherapy-induced premature ovarian failure mice through AMPK/PPAR-gamma/SIRT1 pathway. Sci Rep. 2024;14(1):1447.
25. Dietzel E, Wessling J, Floehr J, Schafer C, Ensslen S, Denecke B, Rosing B, Neulen J, Veitinger T, Spehr M, et al. Fetuin-B, a liver-derived plasma protein is essential for fertilization. Dev Cell. 2013;25(1):106–12.
26. Lechowicz U, Rudzinski S, Jezela-Stanek A, Janciauskiene S, Chorostowska-Wynimko J. Post-translational modifications of circulating alpha-1-Antitrypsin protein. Int J Mol Sci 2020, 21(23).
27. Magyar K. The pharmacology of selegiline. Int Rev Neurobiol. 2011;100:65–84.
28. Qin F, Shite J, Mao W, Liang CS. Selegiline attenuates cardiac oxidative stress and apoptosis in heart failure: association with improvement of cardiac function. Eur J Pharmacol. 2003;461(2–3):149–58.
29. Dean M, Moitra K, Allikmets R. The human ATP-binding cassette (ABC) transporter superfamily. Hum Mutat. 2022;43(9):1162–82.
30. Richardson SJ, Wijayagunaratne RC, D'Souza DG, Darras VM, Van Herck SL. Transport of thyroid hormones via the choroid plexus into the brain: the roles of transthyretin and thyroid hormone transmembrane transporters. Front Neurosci. 2015;9:66.
31. Chen CW, Huang YL, Tzeng CR, Huang RL, Chen CH. Idiopathic low Ovarian Reserve is Associated with more frequent positive thyroid peroxidase antibodies. Thyroid. 2017;27(9):1194–200.
32. Bahri S, Tehrani FR, Amouzgar A, Rahmati M, Tohidi M, Vasheghani M, Azizi F. Overtime trend of thyroid hormones and thyroid autoimmunity and ovarian reserve: a longitudinal population study with a 12-year follow up. BMC Endocr Disord. 2019;19(1):47.
33. Kang MJ, Choi W, Yoo SH, Nam SW, Shin PG, Kim KK, Kim GD. Modulation of inflammatory pathways and adipogenesis by the action of gentisic acid in RAW 264.7 and 3T3-L1 cell lines. J Microbiol Biotechnol. 2021;31(8):1079–87.
34. Razliqi RN, Ahangarpour A, Mard SA, Khorsandi L. Gentisic acid ameliorates type 2 diabetes induced by Nicotinamide-Streptozotocin in male mice by attenuating pancreatic oxidative stress and inflammation through modulation of Nrf2 and NF-small ka, CyrillicB pathways. Life Sci. 2023;325:121770.
35. Parisutham V, Chandran SP, Mukhopadhyay A, Lee SK, Keasling JD. Intracellular cellobiose metabolism and its applications in lignocellulose-based biorefineries. Bioresour Technol. 2017;239:496–506.
36. Chalvatzi S, Papadopoulos GA, Tsiouris V, Giannenas I, Karapanagiotidis IT, Theodoridis A, Georgopoulou I, Fortomaris PD. Dimethylglycine Supplementation in Reduced Energy Broilers' Diets Restores Performance by Improving Nutrient Digestibility. Anim (Basel) 2020, 10(5).
37. Fluhr L, Mor U, Kolodziejczyk AA, Dori-Bachash M, Leshem A, Itav S, Cohen Y, Suez J, Zmora N, Moresi C, et al. Gut microbiota modulates weight gain in mice after discontinued smoke exposure. Nature. 2021;600(7890):713–9.
38. Dhanjal DS, Bhardwaj S, Chopra C, Singh R, Patocka J, Plucar B, Nepovimova E, Valis M, Kuca K. Millennium nutrient N,N-Dimethylglycine (DMG) and its effectiveness in Autism Spectrum disorders. Curr Med Chem. 2022;29(15):2632–51.
39. Ringer KL, McConkey ME, Davis EM, Rushing GW, Croteau R. Monoterpene double-bond reductases of the (-)-menthol biosynthetic pathway: isolation and characterization of cDNAs encoding (-)-isopiperitenone reductase and (+)-pulegone reductase of peppermint. Arch Biochem Biophys. 2003;418(1):80–92.
40. Dieplinger H, Dieplinger B. Afamin–A pleiotropic glycoprotein involved in various disease states. Clin Chim Acta. 2015;446:105–10.
41. Liu J, Huang X, Cao X, Feng X, Wang X. Serum biomarker analysis in patients with premature ovarian insufficiency. Cytokine. 2020;126:154876.
42. Wang X, Chen ZJ. A decade of discovery: the stunning progress of premature ovarian insufficiency research in China. Biol Reprod. 2022;107(1):27–39.
43. Koninger A, Enekwe A, Mach P, Andrikos D, Schmidt B, Frank M, Birdir C, Kimmig R, Gellhaus A, Dieplinger H. Afamin: an early predictor of preeclampsia. Arch Gynecol Obstet. 2018;298(5):1009–16.
44. Pitkanen N, Finkenstedt A, Lamina C, Juonala M, Kahonen M, Makela KM, Dieplinger B, Viveiros A, Melmer A, Leitner I, et al. Afamin predicts the prevalence and incidence of nonalcoholic fatty liver disease. Clin Chem Lab Med. 2022;60(2):243–51.
45. Zheng Y, Zhao F, Hu Y, Yan F, Tian Y, Wang R, Huang Y, Zhong L, Luo Y, Ma Q. LC-MS/MS metabolomic profiling of the protective butylphthalide effect in cerebral ischemia/reperfusion mice. J Stroke Cerebrovasc Dis. 2023;32:107347.
46. Shi W, Deng Y, Zhao C, Xiao W, Wang Z, Xiong Z, Zhao L. Integrative serum metabolomic analysis for preventive effects of Yaobitong capsule in adjuvant-induced rheumatoid arthritis rat based on RP/HILIC-UHPLC-Q-TOF MS. Anal Biochem. 2022;637:114474.

47. Krishna MB, Joseph A, Thomas PL, Dsilva B, Pillai SM, Laloraya M. Impaired arginine metabolism coupled to a defective Redox Conduit contributes to low plasma nitric oxide in polycystic ovary syndrome. Cell Physiol Biochem. 2017;43:1880–92.

Publisher's Note